PHILOSOPHICAL TRANSACTIONS OF THE ROYAL SOCIETY A MATHEMATICAL, PHYSICAL & ENGINEERING SCIENCES

Volcano geodesy: challenges and opportunities for the 21st century

Daniel Dzurisin

Phil. Trans. R. Soc. Lond. A 2000 **358**, 1547-1566
doi: 10.1098/rsta.2000.0603

THE ROYAL SOCIETY

Volcano geodesy: challenges and opportunities for the 21st century

By Daniel Dzurisin

US Geological Survey, David A. Johnston Cascades Volcano Observatory, 5400 MacArthur Boulevard, Vancouver, WA 98661, USA (dzurisin@usgs.gov)

Intrusions of magma beneath volcanoes deform the surrounding rock and, if the intrusion is large enough, the overlying ground surface. Numerical models generally agree that, for most eruptions, subsurface volume changes are sufficient to produce measurable deformation at the surface. Studying this deformation can help to determine the location, volume, and shape of a subsurface magma body and thus to anticipate the onset and course of an eruption. This approach has been successfully applied at many restless volcanoes, especially basaltic shields and silicic calderas, using various geodetic techniques and sensors. However, its success at many intermediate-composition strato-volcanoes has been limited by generally long repose intervals, steep terrain, and structural influences that complicate the history and shape of surface deformation. These factors have made it difficult to adequately characterize deformation in space and time at many of the world's dangerous volcanoes.

Recent technological advances promise to make this task easier by enabling the acquisition of geodetic data of high spatial and temporal resolution from Earth-orbiting satellites. Synthetic aperture radar interferometry (InSAR) can image ground deformation over large areas at metre-scale resolution over time-scales of a month to a few years. Global Positioning System (GPS) stations can provide continuous information on three-dimensional ground displacements at a network of key sites—information that is especially important during volcanic crises. By using InSAR to determine the shape of the displacement field and GPS to monitor temporal changes at key sites, scientists have a much better chance to capture geodetic signals that have so far been elusive at many volcanoes. This approach has the potential to provide longer-term warnings of impending volcanic activity than is possible with other monitoring techniques.

Keywords: volcano geodesy; ground deformation; hazards mitigation; radar interferometry; Global Positioning System

1. Why study volcano deformation?

Volcanoes occur throughout our Solar System and presumably beyond. Earth's crust, oceans, and atmosphere all owe their existence in large part to volcanic activity. Modern or ancient volcanoes occur on all of Earth's major land masses and throughout its ocean basins. Excluding submarine vents, more than 1500 volcanoes have been active on Earth within the past 10 000 years and approximately 50 volcanoes are active in a typical year (Simkin & Siebert 1994, p. 4). The surfaces of other terrestrial planets and planetary moons, notably our own, have been affected by pervasive and, in some

cases, persistent volcanic activity. Io, the innermost moon of Jupiter, produces simultaneous, colossal eruptions from numerous active vents scattered across its surface. It seems safe to say that volcanoes are common features that are essential to life as we know it.

Even so, the fact that volcanoes exist at all is really quite remarkable. Volcanic eruptions are the culmination of a complex series of events that includes the buoyant rise of millions of cubic metres of magma through tens of kilometres of rock—an improbable occurrence by everyday standards. Nonetheless, it happens on Earth and elsewhere surprisingly often.

What is *not* surprising is that the intrusion process profoundly affects both the rising magma and surrounding rock. For example, the confining pressure acting on a body of magma that rises from the base of Earth's crust (*ca.* 30 km depth) to its surface decreases by about four orders of magnitude, from *ca.* 10 kbar to 1 bar. Volatiles such as water, carbon dioxide, and sulphur dioxide that were stable in the magma at depth exsolve and form a separate gas phase as the magma rises and decompresses, probably causing the viscosity of the magma to increase by several orders of magnitude (Lejeune *et al.* 1999). Until the gas bubbles escape, they lower the average density of the magma body and hasten its rise. When the gases *do* escape, assuming they are relatively insoluble in groundwater and therefore can reach the surface (not true for sulphur dioxide, which can be effectively 'scrubbed' by solution in water), they provide an effective means to monitor the intrusion process. By measuring the types and quantities of magmatic gases released as a function of time, scientists can infer the presence of magma recently intruded into the upper crust, its intrusion rate, and approximate depth (see, for example, Gerlach *et al.* 1996).

The effect of the intrusion process on surrounding rock is equally profound. To accommodate intruding magma, the host rock must deform. To appreciate the inevitability of this requirement, consider that 1 km^3 of magma—a volume erupted somewhere on Earth's land surface about once every 10 years (Simkin & Siebert 1994, p. 29)—would occupy a sphere of radius 620 m or a cylinder of radius 100 m extending from the surface to a depth of *ca.* 32 km. Creating space for either body or moving it through the crust is a prodigious task that cannot be accomplished without deforming the host rock.† If the intrusion rate is low enough or the temperature of the host rock is high enough, elastic or ductile deformation occurs and the intrusion process is virtually aseismic. At higher intrusion rates or lower temperatures, brittle failure of the host rock produces numerous earthquakes. It is not uncommon for small earthquakes (most of Richter magnitude $M \leqslant 3$, but a few as large as $M \approx 5$) to occur at rates exceeding one event per minute for hours or days during a rapid, shallow intrusion.

The brittle component of volcano deformation—that is, the part that produces earthquakes—has traditionally been the foundation for most volcano monitoring strategies. As a monitoring target, earthquakes have several advantages over ground deformation. Earthquakes transmit seismic waves that can travel through the solid Earth, so even small events are detectable many kilometres from their source with

† The magnitude of surface deformation could be mitigated in several ways. For example, a large volume of magma might be stored at considerable depth beneath a volcano and then delivered to the surface through a relatively narrow conduit. Or a magma body might develop partly *in situ* by partial melting of host rock, so the net volume change in the vicinity of the body is less than the total volume of magma produced. Regardless of the details, at least *some* deformation of the host rock is inevitable, and models generally agree that the effect should be measurable at the surface in many cases.

relatively inexpensive seismometers. Deformation, in contrast, is a relatively local phenomenon that, until recently, has been measurable only close to its source or farther away only with sophisticated, expensive instrumentation. Also, the inversion of earthquake arrival-time data is a relatively straightforward, three-dimensional geometry problem that can be solved one event at a time for essentially two parameters: earthquake magnitude and location (ignoring path effects). Geodetic inversions generally require data spanning a longer time-interval and with greater spatial density to determine the source location and also distinguish among possible source geometries (sphere, ellipsoid, dyke, fault dislocation). In the absence of spatially dense geodetic data, for example, an *inflating* dyke might not be distinguishable from a *deflating* point source, because both produce localized subsidence. All of these factors combine to make effective geodetic monitoring of volcanoes more difficult than seismic monitoring.

However, earthquake monitoring alone has important limitations at volcanoes. Because earthquakes are local phenomena, no single event provides information about the entire source region. Even the spatial distribution of earthquakes beneath a volcano is inherently ambiguous. Do earthquakes indicate where an intrusion *is* (where deformation of host rock is greatest), or where it *is not* (magma itself does not fracture and is therefore aseismic)? Does an aseismic region beneath a volcano represent magma or hot, 'solid' rock (high-temperature, ductile rock that deforms aseismically under low strain rates)? Might magma be moving aseismically by invading pre-existing fractures or intruding hot, ductile host rock?

These ambiguities can sometimes be resolved with adequate geodetic monitoring. The surface displacement field integrates the effect of the entire intrusion, even if the deformation is partly aseismic. Although steady-state magma movement through established conduits can occur without substantial deformation (e.g. at open-vent systems and during long-lived eruptions), fresh intrusions that precede most eruptions almost inevitably cause surface deformation that 'fingerprints' the intrusion if the surface displacement field can be adequately characterized. This is especially true for intrusions within a few kilometres of the surface, which produce distinctive deformation patterns that reflect the location, size, and shape of the source (Dvorak & Dzurisin 1997). Deeper sources produce less distinctive deformation patterns that contain less information about the shape of the source, but nonetheless reveal its location and size.

No single approach to volcano monitoring (e.g. seismology, geodesy, gas geochemistry) can answer all the questions posed by scientists and residents near a restless volcano. However, when the surface deformation field is measured with sufficient precision and spatial coverage, it constrains the location and quantity of subsurface magma movements far less ambiguously than earthquake locations or gas emission data. Volcano geodesy—by virtue of the high information content of a well-characterized deformation field and the comparatively nascent state of deformation monitoring and modelling techniques—holds a large untapped potential for studying volcanic processes.

2. Why is volcano deformation such an elusive target?

Deformation of host rock is virtually certain during magmatic intrusions, and models indicate that most intrusions are large enough to deform the ground surface by

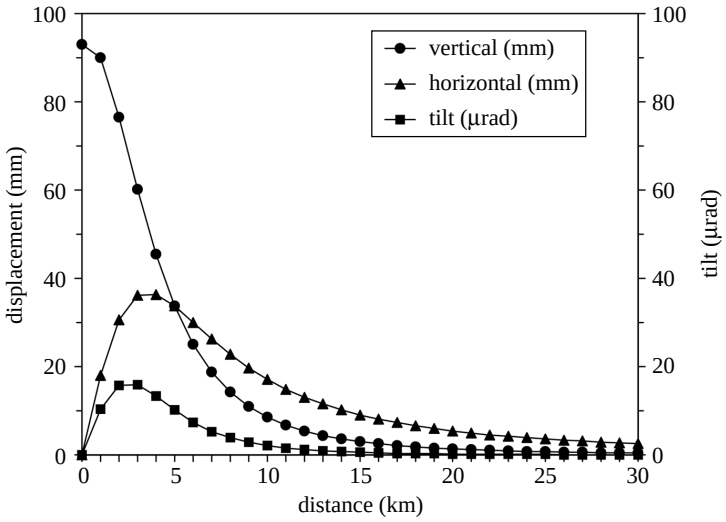

Figure 1. Predicted surface displacements and tilt, as a function of distance r, caused by inflation of a point source deeply buried in an elastic half-space (Mogi 1958). This case represents a source-volume increase $\Delta V = 10^7$ m^3 at a depth $d = 5$ km. According to the model, displacements and tilt scale linearly with volume change. For example, a volume change of 10^8 m^3 would produce displacements and tilts of a factor of 10 greater than shown here.

measurable amounts. Yet, measurements of precursory ground deformation at volcanoes of intermediate composition (e.g. andesite–dacite strato-volcanoes or domes) are relatively rare, except during intense unrest when magma is already close to the surface or after an eruption has begun. This paradox is explained at least in part by a combination of difficult logistics and complexity in the displacement field, in both space and time. By difficult logistics I mean that long repose intervals, difficult access, steep terrain, and limited resources encourage monitoring lapses during which any precursory deformation might escape detection. To appreciate the magnitude of the second factor, consider the complexity inherent in even the simplest model for volcano deformation: a spherical source, deeply buried in an elastic half-space, that changes its volume but not its location as a function of time (Mogi 1958).

Predicted surface displacements for such a source at depth $d = 5$ km that increases in volume by 10^7 m^3 are shown in figure 1. This case corresponds to a 'moderate' to 'moderate-large' eruption with a volcanic explosivity index (VEI) of 2 or 3 (Simkin & Siebert 1994, p. 23). The maximum predicted surface displacements (vertical, $\Delta Z_{\max}$; horizontal, $\Delta X_{\max}$; tilt, $\Delta\tau_{\max}$) are $\Delta Z_{\max} = 95$ mm at distance $r = 0$ km (directly above the source), $\Delta X_{\max} = 37$ mm at $r = 3.5$ km, and $\Delta\tau_{\max} = 16$ μrad at $r = 2.5$ km. According to the model, these results scale linearly with volume change. So a volume change of 10^9 m^3 (corresponding to a 'large' or 'very large' eruption with a VEI of 4–5) would produce maximum displacements and tilts 100 times larger than those shown in figure 1, and a volume change of 10^6 m^3 ('small' to 'moderate' VEI of 1–2) would produce displacements and tilts 10 times smaller.†

† All such calculations reported here assume a Poisson's ratio of $\nu = 0.25$ for the host rock, which corresponds to the case in which the uplift volume is a factor of 1.5 times greater than the injected volume. For a discussion of the dependence of surface displacements on ν, see Delaney & McTigue (1994).

Taken at face value, these results seem encouraging. Even a small volume change of 10^6 m^3 at $d = 5$ km might be detectable with state-of-the-art geodetic techniques ($\Delta Z_{\max} = 9.5$ mm, $\Delta X_{\max} = 3.7$ mm, and $\Delta\tau_{\max} = 1.6$ μrad). For volume changes of 10^7 m^3 or larger, which correspond to volumes erupted during most hazardous eruptions, surface deformation should be measurable even with classical geodetic instruments that are widely used for volcano monitoring (e.g. theodolite, EDM, bubble tiltmeters).

However, at least three factors combine to make such measurements more difficult in practice than implied by the model results. First, the spatial resolution of most geodetic datasets at strato-volcanoes is inadequate for the task at hand. This shortcoming can be caused by difficult access (remote location, rugged terrain, high elevation, dense vegetation), unacceptable hazards to personnel in proximal areas during periods of unrest, or limited resources (time, equipment, money, personnel). Second, the temporal resolution of most geodetic datasets is also inadequate, for some of the same reasons listed above and also because monitoring programmes are difficult to maintain during typically long repose intervals when little seems to be happening at the volcano. Finally, some geodetic techniques used to monitor volcanoes are not sufficiently precise to detect small surface changes that might precede many eruptions. In short, complete characterization of volcano deformation requires that measurements be made in the right place, at the right time, and with adequate precision—a difficult challenge using conventional geodetic techniques.

All three limiting factors played a role at Mt St Helens before its large eruption on 18 May 1980. A brief review of that experience illustrates the difficulties faced by scientists trying to measure volcano deformation during a crisis, and also the potential of new space-based geodetic techniques for characterizing deformation in space and time. With remarkable foresight, D. A. Swanson first measured a 7.6 km EDM line from Smith Creek Butte to East Dome in 1972, in the 115th year of quiescence at Mt St Helens since the end of its previous eruption in 1857. The line was next measured on 10 April 1980, three weeks after the onset of an intense swarm of earthquakes beneath the volcano. In hindsight, the earthquakes were caused by the intrusion of a cryptodome, which caused the volcano's north flank to bulge outward at rates of 1.5–2.5 m d^{-1} before the edifice failed catastrophically on May 18 to produce the largest landslide in recorded history (Lipman *et al*. 1981).

In the preceding 8 years, the line between Smith Creek Butte and East Dome had contracted just 16 mm—less than the uncertainty in the measurement. The line was remeasured on 25 April 1980 (+15 mm), and again after the 18 May 1980, eruption (−18 mm). At the same time, repeated surveys of a local geodetic network (theodolite and EDM) established at the volcano in April 1980 revealed intense deformation of the volcano's north flank but only small changes elsewhere on the edifice (as much as 2.5 m d^{-1} versus a few mm d^{-1}). The authors concluded that ' ... except for the bulge (on the volcano's north flank), Mount St. Helens was geodetically stable during this period' (Lipman *et al*. 1981, p. 151).

The virtual absence of measured ground deformation beyond a 1.5 km × 2 km bulge on the north flank of Mt St Helens during the two months preceding the 18 May 1980, eruption is partly attributable to each of the three factors listed above. First, consider the EDM results for the line from Smith Creek Butte to East Dome. The essentially null result from 1972 to 10 April 1980, is the only geodetic measurement that began before the onset of intense, shallow seismicity on 20 March 1980. With

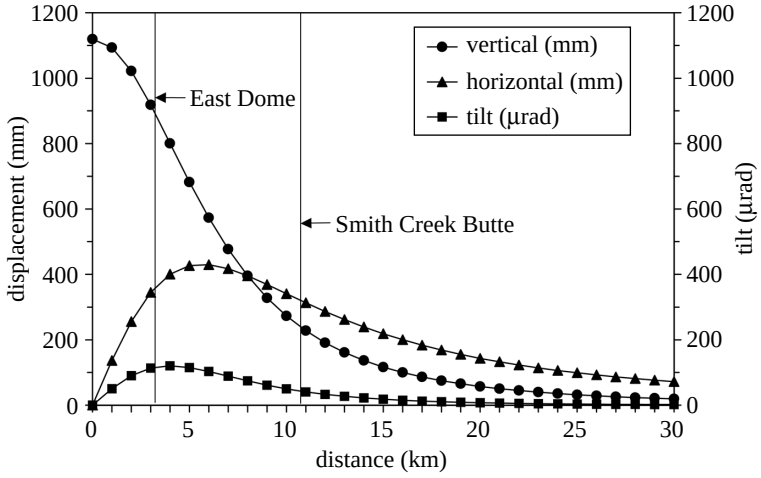

Figure 2. Surface displacements and tilt predicted by an elastic, point-source model (Mogi 1958) for the case of a source-volume increase $\Delta V = 3 \times 10^8$ m^3 at depth $d = 8$ km. These values correspond to the erupted volume (magma equivalent) and source depth for the 18 May 1980 eruption at Mt St Helens. Also shown are the locations of two EDM stations, East Dome and Smith Creek Butte, at radial distances $r = 3$ km and 10.5 km, respectively, from the volcano's summit. The line length between those stations was measured in 1972 and several times in 1980, with null results. The model predicts relatively large horizontal displacements at both stations, but very little relative movement between them.

the benefit of hindsight, let's first consider whether this measurement was made in the 'right place'. To a large degree, the right place is determined by the depth of the deformation source. From the distribution of earthquake hypocentres for the period immediately following the onset of the 18 May 1980 eruption, Scandone & Malone (1985) concluded that the source depth for magma erupted that day was 7–14 km. Rutherford *et al*. (1985) based their independent estimate of the source depth, 7.2 ± 1 km, on the mineral phase assemblage found in 18 May pumice and experimentally determined phase equilibria. Here, I assume a source depth of 8 km and an erupted volume of 0.3 km^3 (Pallister *et al*. 1992, p. 129).

Surface displacements predicted by the same elastic, point-source model discussed above for the case of $\Delta V = 0.3$ km^3 and $d = 8$ km are shown in figure 2, together with the relative locations of East Dome ($r = 3$ km) and Smith Creek Butte ($r = 10.5$ km). At those locations, the model predicts large, but essentially equal, horizontal displacements (344 mm and 327 mm, respectively). As a result, the distance between East Dome and Smith Creek Butte would change very little—less than the EDM measurement uncertainty. So, in hindsight, the EDM measurements made in 1972 and 1980 might have been relatively insensitive to volume changes in the 8 km-deep magma body that fed the 18 May 1980 eruption. As a result, substantial ground displacements could have gone undetected.

Of course, it is also possible that such displacements did not occur and the source of the discrepancy between EDM measurements and modelling results is an inappropriate model. This might be the case if most of the magma that erupted on 18 May 1980, accumulated in the crust before the first EDM measurements in 1972 and therefore the volume change used in the model is too large (see below). Alternatively,

the deformation field might not have been radially symmetric, perhaps because the material properties of the crust beneath the volcano were inhomogeneous. On the other hand, the discrepancy is not easily explained by an inappropriate source geometry nor Poisson's ratio, because these factors have relatively small effects on the surface displacement field except for very shallow sources (McTigue 1987; Delaney & McTigue 1994). My point is not to defend the use of the Mogi model in this case, but rather to point out that its results cannot be discounted on the basis of available information. The absence of relative motion between Smith Creek Butte and East Dome is permissive of the interpretation based on the model that those stations experienced large, but nearly equal, absolute displacements that escaped detection.

Before moving on to other factors that might have influenced the EDM results at Mt St Helens, consider what other guidance can be taken from the model illustrated in figure 2. Vertical displacements exceed horizontal displacements by a factor of three or more in proximal areas ($r < 3$ km). This suggests that height-change measurements near the summits of volcanoes should receive high priority, at least during periods of quiescence. Unfortunately, many summit areas are inhospitable to both human observers and *in situ* monitoring instruments, which makes such measurements difficult to acquire. For measurements of horizontal displacements, an implication of the model is that both proximal ($r < 3$ km) and distal ($r > 20$ km) stations are essential to adequately measure deep-seated deformation. Investing in such an expansive network might seem ill-advised with limited resources, but it offers the potential to detect deep-seated magmatic deformation and thus to provide longer-term warning of impending volcanic activity than is possible otherwise. A final observation from figure 2 is that ground tilt is fraught with the same inherent ambiguity as horizontal displacement: the same amount occurs at two different radial distances. This means that tiltmeter arrays, like EDM or other horizontal networks, must be spatially dense *and* extensive to adequately characterize the deformation field in the absence of other information about its shape and extent.

There are at least two other explanations for the null results between East Dome and Smith Creek Butte from 1972 to 1980, which correspond to the other two complicating factors mentioned above. First, consider the possibility that the EDM measurements were made at the wrong time. If, for example, the 0.3 km^3 of magma erupted on 18 May 1980, accumulated at a constant rate from 1857 to 1980, then 93% of it had already arrived at 8 km depth before the first EDM measurement was made in 1972. The arrival of the final 7% between 1972 and 1980 could easily have gone undetected, especially if the Smith Creek Butte–East Dome line was insensitive to volume changes at 8 km depth.

The importance of making frequent geodetic measurements, even during periods of apparent quiescence, is illustrated by the results of repeated levelling surveys across the Yellowstone caldera, Wyoming, from 1976 to 1998 (see figure 3). Results of successive surveys revealed a consistent pattern of uplift from 1976 to 1984, subsidence from 1985 to 1995, and renewed uplift from 1995 to 1998, all with respect to a datum on the southeast caldera rim (Dzurisin *et al*. 1994, 1999). In each case, the largest displacements occurred near benchmark DA3, located in the central part of the caldera near Le Hardy Rapids. The net height change at DA3 from 1976 to 1998 was only 10 ± 5 mm, which corresponds to an average uplift rate of 0.5 ± 1 mm yr^{-1}. On the other hand, intervening surveys reveal that DA3

(1) rose 176 ± 5 mm from 1976 to 1984 (22 ± 1 mm yr^{-1}),

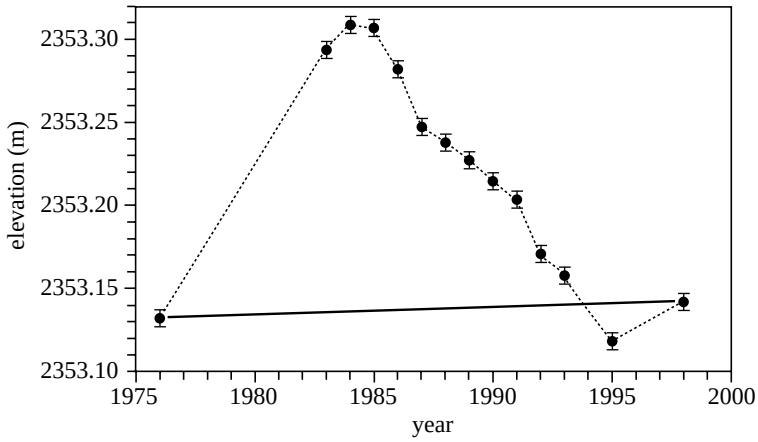

Figure 3. Height changes as a function of time at benchmark DA3 near Le Hardy Rapids, Yellowstone caldera, measured by repeated levelling surveys (Dzurisin *et al*. 1999). Changes shown are relative to benchmark 36 MDC, located *ca*. 23 km southeast of DA3 at Lake Butte, along the caldera rim. Maximum uplift and subsidence along a levelling traverse across the caldera consistently occurred near Le Hardy Rapids. Solid line represents the displacement history that probably would have been inferred from just the surveys in 1976 and 1998. Dashed line represents a more accurate, but still incomplete, history based on results of 14 surveys conducted during that interval.

(2) moved very little from 1984 to 1985 (-2 ± 1 mm yr^{-1}),

(3) subsided -188 ± 5 mm from 1985 to 1995 (-19 ± 1 mm yr^{-1}) at rates that varied from year to year between -9 ± 1 mm yr^{-1} and -35 ± 1 mm yr^{-1}, and

(4) rose 24 ± 1 mm from 1995 to 1998 (8 ± 1 mm yr^{-1}).

Clearly, infrequent surveys can produce a very distorted view of actual ground movements, especially if the displacement rate changes appreciably with time. The EDM measurements at Mt St Helens in 1972 and April 1980, for example, could be analogous to the Yellowstone levelling surveys in 1984 and 1985—poorly timed to capture deep-seated inflation that might have occurred between 1857 and 1972.

A third factor that might have played a role in the null results at Mt St Helens is the detection threshold for sparse (in both time and space) EDM measurements relative to the amount of ground deformation that may have occurred from 1972 to April 1980. Lipman *et al*. (1981, pp. 148 and 151) estimated the uncertainty of their EDM measurements at Mt St Helens to be ±10 mm over distances of 2–4 km, and concluded that line-length changes of the order of +16 mm to −18 mm measured on the 7.5 km line from Smith Creek Butte to East Dome were insignificant. As shown above, a Mogi-type model predicts only 17 mm of relative horizontal displacement between Smith Creek Butte and East Dome for the case of 0.3 km^3 of magma intruded at 8 km depth. Of course, the relative motion would be even smaller if some of the magma that erupted on 18 May 1980 arrived at 8 km depth before 1972. Alternatively, the Mogi model results might be misleading and precursory deformation might have been mostly limited to the north flank bulge. In hindsight, though, various factors could have conspired to make the Smith Creek Butte–East Dome EDM measurements insensitive to the accumulation of magma several kilometres beneath Mt St Helens.

A more effective approach might have been to focus on vertical deformation, even though vertical-angle measurements by theodolite are inherently less precise than EDM measurements over the distances involved at Mt St Helens. For example, Lipman *et al*. (1981, p. 148) estimated the uncertainty of their theodolite measurements to be ±5–10 seconds of arc, which corresponds to ±18–36 cm over the 7.5 km distance from Smith Creek Butte to East Dome. The same Mogi model that predicts only 17 mm of relative horizontal movement between those points predicts 670 mm of relative vertical movement (see figure 2). A change of that magnitude might have been resolvable by theodolite in 1980, and now would easily be measurable with GPS or InSAR.

3. Space-based geodetic techniques

Whereas the preceding section emphasized some of the limitations of classical geodetic techniques for volcano monitoring, henceforth my focus will be on the advantages of two relatively new, space-based geodetic techniques: GPS and InSAR. I do not mean to imply that remote sensing techniques should replace conventional geodetic measurements at volcanoes. On the contrary, several decades of experience have shown that the best approach is to combine several techniques, each with its own strengths and weaknesses, to obtain as complete a picture of the deformation field as possible. Granted that the EDM, theodolite, level, strainmeter, and tiltmeter will continue to play an important role in volcano monitoring for years to come, GPS and InSAR offer some unique capabilities that can help identify and track deformation that might otherwise be missed. In the context of the foregoing discussion, the best way to avoid making geodetic measurements at the wrong place or time is to make them everywhere, all the time. Fortunately, InSAR and GPS go a long way toward making that goal achievable.

(*a*) *Synthetic aperture radar interferometry*

A limitation shared by virtually all conventional geodetic techniques is that they produce point-to-point information that is almost always too sparse to characterize adequately the shape and extent of the deformation field. For example, the geodetic network established at Mt St Helens starting in mid-April 1980 consisted of 21 stations comprising 19 lines in an area of *ca.* 300 km^2 (Lipman *et al*. 1981, p. 147). The closest and farthest stations from the summit of the volcano were at distances of *ca.* 1 km and 10 km, respectively. At most volcanoes, existing geodetic networks are considerably less dense. From the foregoing discussion, it should be clear that no practical geodetic network that relies on point-to-point measurements will be adequate to distinguish among the large number of potential deformation sources (ellipsoid, slab, dislocation) that might combine to deform a volcano and its surroundings, especially given the fact that the location, depth, geometry, and sign (i.e. inflation or deflation) of each contributing source are unknown. The only hope, it would seem, is some magical technique capable of measuring an extremely dense network of points to produce a detailed 'snapshot' of the entire displacement field. Until a few years ago, such a technique was a flight of fancy. Now, it has a name: InSAR.

InSAR is a remote sensing technique that has received considerable attention from Earth scientists since it was used by Massonnet *et al*. (1993) to reveal the surface dis-

placement field caused by the magnitude 7.3 Landers earthquake centred *ca.* 150 km east of Los Angeles, California, on 28 June 1992. The principles and applications of radar interferometry have been described elsewhere (Massonnet & Feigl 1998) and are beyond the scope of this paper. A key point is that InSAR is capable of producing a detailed image of the surface displacement field, rather than measurements at only a small number of fixed points. The resulting snapshot portrays the component of ground motion in the satellite look direction with centimetre-scale precision, over lateral dimensions of tens of kilometres, without a requirement for ground access to the field area, even at night or in bad weather—close enough to magic for our purposes. Three examples will serve to illustrate the power of InSAR for studying volcano deformation.

(*b*) *Yellowstone*

As noted above, repeated levelling surveys at the Yellowstone caldera, Wyoming, have tracked periods of uplift and subsidence at average rates of 1–2 cm yr^{-1} since 1923 (Dzurisin *et al.* 1994). Only three surveys of the entire Yellowstone levelling network have been made during the 20th century, in 1923, 1975–77, and 1987. Starting in 1983, a much smaller levelling traverse across the caldera was measured in most years to keep track of what was assumed to be a spatially consistent displacement field (along the frequently measured traverse, the pattern of subsidence seemed to mirror the pattern of uplift).

A three-year lapse in the levelling surveys from 1995 to 1998 set the stage for two surprising discoveries made by the first InSAR study of Yellowstone. Wicks *et al.* (1998) produced several radar interferograms of the Yellowstone region from European Space Agency ERS-1 and ERS-2 C-band ($\lambda = 5.6$ cm) radar images (see figure 4). Each radar image covers an area on the ground of *ca.* 100 km × 100 km, so the entire caldera and its immediate surroundings are included in each image. Most of the Yellowstone region is forested and also subject to heavy winter snowpack that lingers at higher elevations into June or July. Both factors contribute to loss of coherence in C-band radar images, which is manifested in the interferograms as areas of random phase. Surprisingly, most of the Yellowstone region proved to be coherent enough, at least for summer scenes separated by up to two years, to be useful for mapping surface displacements.

The earliest interferogram, for the period from August 1992 to June 1993 (see figure 4*a*), confirmed what was already known from levelling surveys in the eastern part of the caldera: an area of subsidence centred north of Yellowstone Lake and near the Sour Creek resurgent dome. The first surprise came from the next sequential interferogram, for the period from June 1993 to August 1995 (see figure 4*b*), which revealed that the centre of subsidence had shifted to the western part of the caldera, near the Mallard Lake resurgent dome. Earlier levelling surveys had not detected any migration in the deformation pattern, probably because the complete surveys were too infrequent and because the annual surveys covered only the eastern part of the caldera. The second surprise is contained in the third and fourth interferograms, which captured the resumption of uplift in 1995 following more than a decade of steady subsidence (as measured by levelling). From August 1995 to September 1996, a relatively small area near the Mallard Lake dome continued to subside, while part of the Sour Creek dome began to rise for the first time since 1984 (see figure 4*c*).

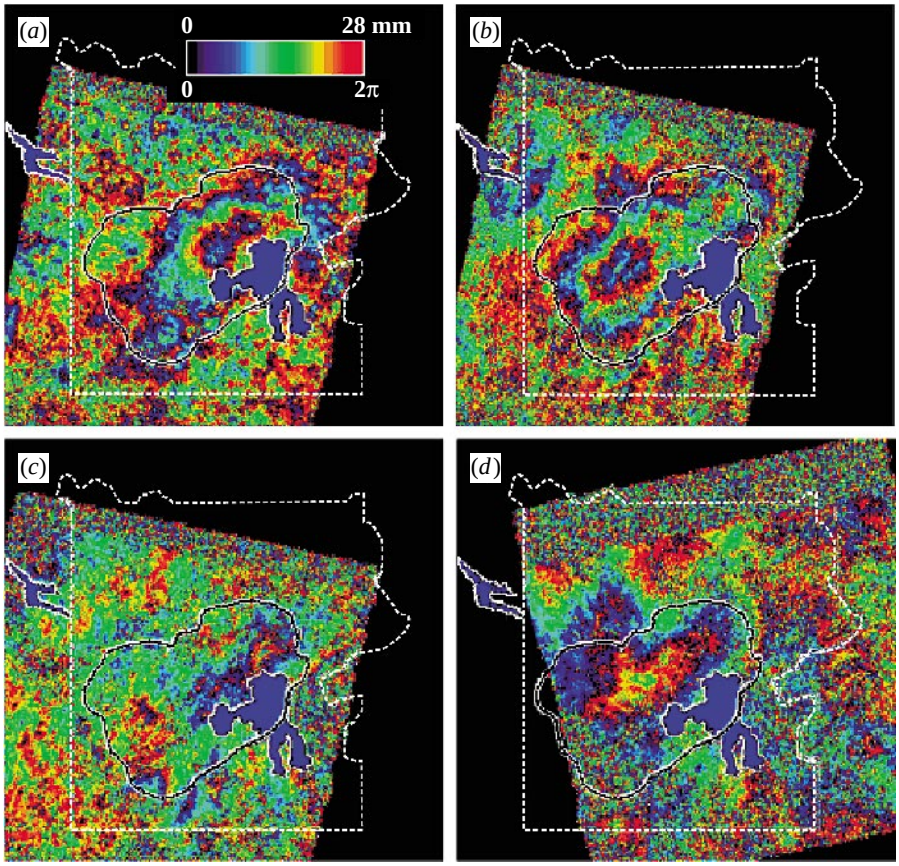

Figure 4. Four interferograms of the Yellowstone region produced by Wicks *et al*. (1998) from ERS-1 and ERS-2 radar images. White, dashed line represents the boundary of Yellowstone National Park; solid black line outlines Yellowstone caldera. The range of colours shown in the colour bar corresponds to one cycle of phase change from 0 to 2π (one fringe). Each fringe represents 2.83 cm of range change between a point on the ground and the satellite. The colour sequence blue–green–yellow–red represents increasing range from satellite to ground (i.e. subsidence of the ground). Note that the opposite colour scheme is used in figures 5–7. The first three interferograms are sequential, whereas the time periods covered by the third and fourth overlap. (*a*) August 1992 to June 1993: this image shows over 30 mm of subsidence centred in the northeastern half of the caldera in the vicinity of the Sour Creek resurgent dome. (*b*) June 1993 to August 1995: the centre of subsidence (*ca.* 40 mm maximum) has shifted in this image to the southwestern half of the caldera near the Mallard Lake resurgent dome. (*c*) August 1995 to September 1996: the fringe pattern in the northeastern half of the caldera in this image corresponds to *ca.* 20 mm of uplift in the vicinity of the Sour Creek dome (note the reversed colour sequence toward the centre of the fringe pattern relative to (*a*) and (*b*)). (*d*) July 1995 to June 1997: in this image, uplift extends throughout the central part of the caldera (maximum *ca.* 30 mm).

By June 1997, uplift had spread throughout most of the caldera (see figure 4*d*). The resumption of uplift in the eastern part of the caldera was confirmed by a levelling survey in 1998 (Dzurisin *et al*. 1999). Wicks *et al*. (1998) inferred that

the displacements revealed in the interferograms were caused by lateral migration of hydrothermal or magmatic fluid into and out of two sill-like bodies located *ca.* 8 km beneath the caldera floor.

(*c*) *Akutan volcano*

An even more striking demonstration of InSAR's ability to map complex surface displacements at volcanoes is available for Akutan, a composite strato-volcano situated in the west-central part of Akutan Island in the eastern part of the Aleutian volcanic arc. Akutan is one of the most active volcanoes in the Aleutian volcanic arc. At least 27 separate eruptive episodes have been noted since 1790, and additional events have probably gone unrecorded (Miller *et al*. 1998). Most of the reported eruptions included small-to-moderate (VEI of 2) explosions from an active intracaldera cone. The most recent eruptive activity was a series of small (VEI of 1) steam and ash emissions during March–May 1992.

Beginning early on 11 March 1996, Akutan Island was struck by an intense swarm of earthquakes that lasted *ca.* 11 h (Lu *et al*. 2000*a*). The swarm consisted of more than 80 earthquakes greater than magnitude 3.5 ($M_{\max} = 5.1$). A second, more vigorous swarm on March 14 lasted *ca.* 19 h and included more than 120 earthquakes greater than magnitude 3.5. Thousands of smaller earthquakes also occurred during these periods of strong activity, including roughly 3000 felt by local residents. Fresh ground cracks discovered in July 1996 almost surely formed during the March earthquake swarms. The most extensive cracks occurred in a zone roughly 250 m wide and 3 km long northwest of Akutan caldera (see figure 5). Local graben structures with vertical displacements of 30–80 cm suggest that these cracks formed in response to tumescence of the volcano's northwest flank. On the east side of the island, cracks a few centimetres wide apparently represent activation of Holocene normal faults (Richter *et al*. 1998).

Interferograms of Akutan Island for periods that include the March 1996 earthquake activity reveal a complicated pattern of ground displacements centred near Akutan caldera and extending across most of the island (Lu *et al*. 2000*a*; see figure 5). The most intense deformation occurred on the northwest flank of Akutan volcano, where more than 21 interferometric fringes are discernible between the coastline and the upper flank (the summit area itself is incoherent as a result of perennial snow and ice). Each fringe represents 2.83 cm (half the radar wavelength) of range change along the satellite look direction. The look angle of the ERS satellites is *ca.* 22° from vertical, so interferograms formed from ERS images are sensitive mostly to vertical ground movements. In this case, the fringe pattern indicates that the upper northwest flank of the volcano moved *toward* the satellite vantage point (mostly up) by at least 60 cm relative to the coastline in that area. Similarly, there are more than eight fringes southwest of the caldera, which indicate that the upper southwest flank moved up at least 23 cm relative to the area marked by the lowermost fringe in that area. The southwest coastal zone is incoherent, so any additional deformation that might have occurred there is unknown.

The pattern of surface displacements is distinctly different on the eastern half of the island. Loss of coherence except in several isolated areas makes the pattern more difficult to discern, but Lu *et al*. (2000*a*) concluded that the area east of Akutan volcano subsided along an axis roughly coincident with the trend of ground cracks that formed in March 1996.

Lu *et al*. (2000*a*) modelled the surface displacements revealed by two independent Akutan interferograms as the net effect of four distinct sources (see figure 6):

(1) a dyke dipping 50° N16° E and striking N74° W that opened to within 0.9 km of the surface beneath the northwest flank of the volcano;

(2) a Mogi-type source *ca.* 7 km beneath the west flank that inflated by *ca.* 0.09 km^3 and presumably fed the dyke described above;

(3) a deflation source beneath the east part of the island, modelled as a steeply dipping, contracting dyke; and

(4) another deflation source, similar to (3) but located beneath the west flank of Akutan volcano.

The fourth source is required to account for certain details of the interferograms at the west end of the island.

For this paper, the specific modelling results are less important than the general observation that InSAR is capable of providing geodetic information with sufficient spatial resolution and coverage to support detailed interpretation of multiple deformation sources. Although the meaning of the four sources shown in figure 6 in terms of physical mechanisms is open to discussion, it is clear from the complexity of the interferograms that no single source mechanism is likely to account satisfactorily for the observations. It is also clear that point-to-point geodetic measurements, even if they had been made at Akutan before the March 1996 earthquake activity, could not have captured the full complexity of the displacement field revealed by the interferograms. The lesson from Akutan is that, when seismic or other unusual activity near a volcano attracts attention to a specific time period, InSAR can in some cases provide a remarkably detailed map of the spatial extent and character of the displacement field. A larger challenge for InSAR is to identify volcanoes that may be deforming in the absence of other signs of unrest, which would allow scientists to intensify their monitoring efforts and hopefully provide longer-term warnings of impending eruptive activity. Recently, there has been an exciting development in this regard.

(*d*) *Westdahl volcano*

Westdahl volcano is located on Unimak Island in the eastern Aleutian arc, *ca.* 85 km southwest of the tip of the Alaska Peninsula and 100 km northeast of Akutan Island. Known eruptions of Westdahl occurred in 1964, 1978, and 1991–92. The 1991–92 eruption, which began on 29 November 1991, from a fissure through ice, produced a lava flow that extended *ca.* 7 km down the northeast flank, debris flows that reached the sea 18 km from the vent, and ash plumes to 7 km altitude. Activity declined in mid-December and had ceased by mid-January 1992 (Miller *et al*. 1998, pp. 45–46). A five-station seismic network was installed at Westdahl volcano by the Alaska Volcano Observatory in July 1998.

Motivated primarily by eruptions at nearby Shishaldin volcano in 1995–96 and early 1999, Lu *et al*. (2000*b*) produced interferograms for Unimak Island that span the interval from 1992 to 1998 and made a surprising discovery. Unheralded by unusual activity of any kind, Westdahl volcano began to re-inflate almost immediately after the end of its most recent eruption in early 1992 (see figure 7). Several independent

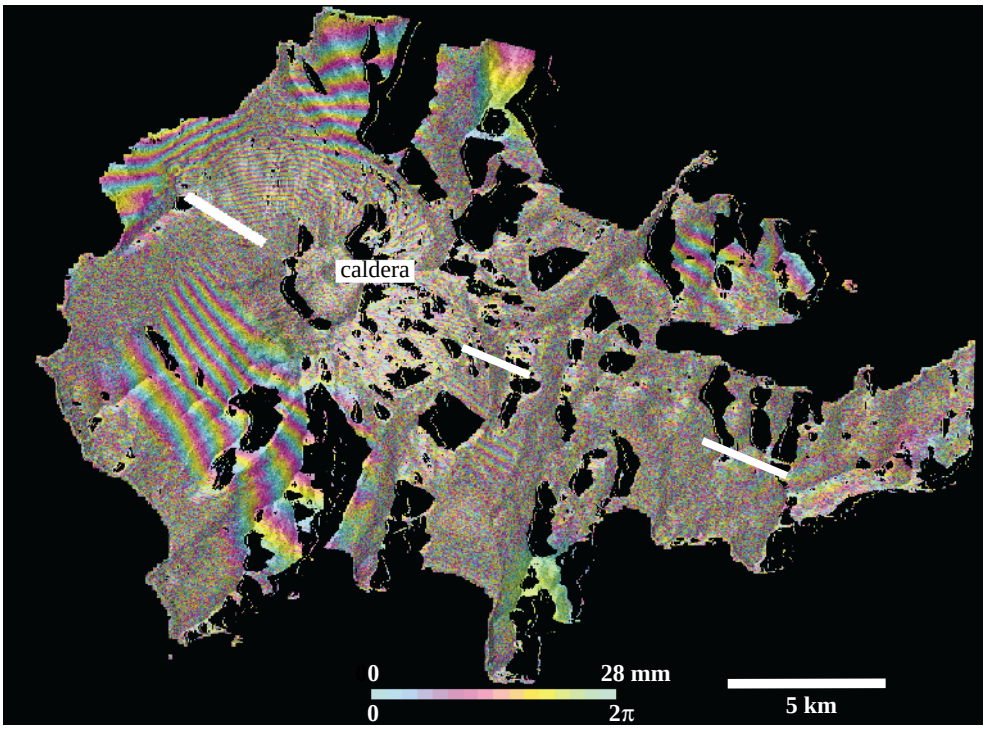

Figure 5. Radar interferogram of Akutan Island for the period from 20 August 1993 to 7 October 1996, from Lu *et al*. (2000*a*). Each fringe (complete colour cycle as shown in bar at bottom) represents 2.83 cm of range change in the satellite look direction. In this case, the colour sequence blue–green–yellow–red represents *decreasing* range from satellite to ground (i.e. uplift of the ground). Note that the opposite colour scheme is used in figure 4. Dark regions indicate areas with severe geometric distortion in the SAR images caused by steep slopes. Akutan volcano and its summit caldera are situated in the west-central part of the island; the eastern part consists mainly of deposits from ancestral Akutan volcano and older, undifferentiated volcanic rocks (Richter *et al*. 1998). Bold line northwest of Akutan caldera represents a 250 m-wide zone of ground cracks that formed during the March 1996 earthquake swarm. Two other lines southeast of the caldera represent cracks that formed along Holocene normal faults.

interferograms reveal a consistent pattern of uplift centred beneath the east flank of the volcano. A preliminary, best-fit model of the displacement field includes a Mogi-type source located 8–9 km beneath Westdahl that inflated by *ca.* 0.05 km^3 from 1992 to 1998 (Lu *et al*. 2000*b*).

The Westdahl result is especially important for two reasons. First, this may be the first time that InSAR has revealed inflation of an otherwise quiescent volcano for several years before an eventual eruption. This raises the possibility that InSAR can be used to 'prospect' for volcanic systems where magma is accumulating before other signs of unrest are recognized. If so, scientists can take advantage of the advance information to intensify their monitoring efforts at inflating volcanoes and provide longer-term warnings to those who might be affected by future eruptive activity. Second, the inflation sources beneath Westdahl and Akutan are relatively deep, which means that InSAR can be used to identify deforming magma bodies even at mid-

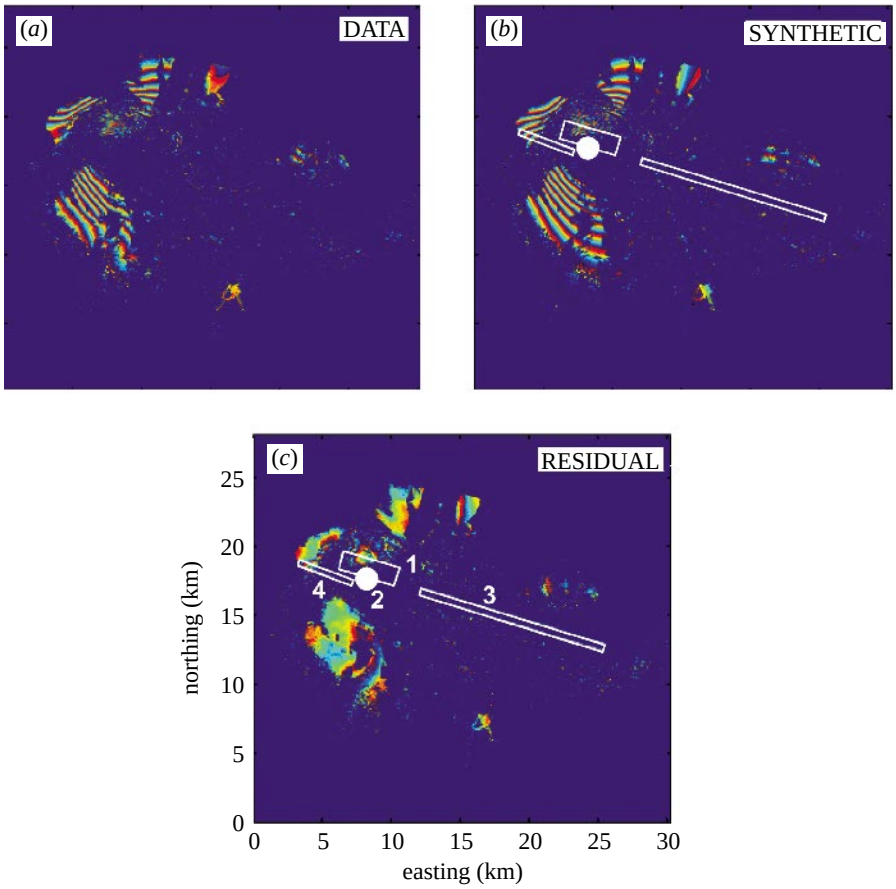

Figure 6. Interferogram and modelling results for Akutan Island, from Lu *et al.* (2000*a*). (*a*) Observed deformation interferogram, with low-coherence areas masked out. (*b*) Synthetic deformation interferogram from best-fitting model. (*c*) Residual interferogram showing the difference between (*a*) and (*b*). The surface projections of four modelled sources are shown as three white polygons and a circle in (*b*) and (*c*). Sources: 1, shallow, dipping dyke (expanding); 2, Mogi-type source (expanding); 3 and 4, steeply dipping dykes (contracting). Each fringe (complete colour cycle) represents 2.83 cm of range change in the satellite look direction. Colour scheme is the same as in figure 5.

crustal depths, before they rupture toward the surface to generate seismic activity and feed shallow intrusions or eruptions.

Clearly, InSAR can provide remarkably detailed images of volcano deformation, even at seemingly quiescent volcanoes where magma is accumulating at considerable depth. On the other hand, the technique is subject to several limitations and error sources that reduce its usefulness in some situations. The most serious of these is loss of coherence between radar images (also called 'decorrelation'). This results from changes in the surface that alter its radar-reflective properties to the extent that the interferometric effect is lost (Massonnet & Feigl 1998). Vegetation changes, erosion or deposition of surface material, changes in snow or ice cover, and soil moisture changes can all cause decorrelation in parts or all of an interferogram.

Less serious but nonetheless worrisome are artefacts caused by spatial and temporal variations in the ionosphere or troposphere. Variations in the ionospheric electron density or in the tropospheric water vapour concentration affect the refractive index for radar waves, which in turn affects the phase of the surface-reflected radar signal. The resulting phase changes produce fringes in interferograms that could be mistaken for surface deformation. The same is true for topographical errors in a digital elevation model (DEM) used to produce an interferogram. Fortunately, each of these error sources has distinctive characteristics that allow the resulting artefacts to be identified in most cases (Massonnet & Feigl 1998). For example, artefacts caused by ionospheric or tropospheric variations are ephemeral and therefore will not appear in the same form in two interferograms made with different sets of images. On the other hand, spurious fringes caused by topographical errors in a DEM will be common to all interferograms based on that DEM, but the magnitude of the error will change with the changing viewing geometries among different sets of radar images.

Yet another limitation of InSAR is the relatively long orbital repeat times for existing SAR satellites. For example, the minimum repeat time for ERS radar images is currently 35 days, and at many volcanoes where seasonal changes cause coherence loss in C-band radar images, the minimum practical repeat time is about one year (typically summer to summer). An annual repeat cycle can be very useful for some types of volcano studies, including the three cases described above, but during a volcanic crisis much more frequent geodetic measurements are needed to help assess a rapidly evolving and potentially hazardous situation.

Fortunately, several types of sensors are capable of producing essentially continuous information about volcano deformation, including strainmeters, tiltmeters, and continuous GPS stations. The very high precision of borehole volumetric strainmeters makes them especially useful for monitoring strain changes caused by subvolcanic intrusions, even tens of kilometres from the source (Linde *et al*. 1993). Especially if the siting of such instruments can be guided by InSAR results that reveal the shape of the displacement field during an early phase of volcano unrest, continuous sensors can provide invaluable information about the temporal evolution of activity. One such technique, continuous GPS, has recently matured to the point that it is being used at a steadily increasing number of volcanoes worldwide. The following discussion serves to illustrate the utility of continuous geodetic monitoring at volcanoes, whether by GPS or other types of instruments such as strainmeters or tiltmeters.

(*e*) *Continuous GPS: an example*

As the cost of high-precision GPS receivers has steadily decreased by more than an order of magnitude over the past decade, networks of continuously recording GPS stations have become more extensive and commonplace. Two notable examples are GEONET, a nationwide GPS network in Japan that includes more than 900 stations, and SCIGN, the Southern California Integrated GPS Network that will eventually include about 250 stations. Smaller networks of receivers have been installed at several volcanoes around the world, including Kilauea, Mauna Loa, Augustine, Yellowstone, Long Valley, Popocatepetl, Taal, and several volcanoes in Japan. Most of these networks comprise fewer than a dozen stations, which means that other types of geodetic measurements are necessary to place the GPS data in context.

Within the boundaries of Yellowstone National Park, five continuous GPS stations were operating at the end of 1999, and there are plans to expand the network to about

a dozen stations within the next few years (see figure 8).† The design of the network illustrates the advantage of having InSAR observations available to guide the siting of continuous GPS stations. Based on the Yellowstone interferograms described above, we determined that the Sour Creek and Mallard Lake resurgent domes were key localities for continuous monitoring, and that migration of the deformation centre could be monitored effectively by a third continuous station located between those two sites. Accordingly, three continuous stations were added to the Yellowstone network in September 1999—one on each of the domes and one in Hayden Valley, midway between the two domes. Some of the interferograms also suggested anomalous motion near Norris, along the north caldera rim, and the Hebgen Lake fault zone, immediately northwest of the caldera. Two additional GPS stations are planned for installation in those areas in 2000. The remaining stations shown in figure 8 are intended to monitor areas with persistent seismicity and to provide ties to more distant stations.

The important point here is that neither InSAR nor continuous GPS can provide all of the information needed to track and understand ground motions at Yellowstone. Repeated levelling surveys revealed periods of uplift and subsidence within the caldera, but failed to detect lateral migration of the deformation centre. InSAR showed that the deformation centre migrates on time-scales of a year or less, but currently is not useful over time-scales of less than a month. Continuous GPS stations provide data that can be analysed on a daily, hourly, or shorter basis, but even with modern, relatively inexpensive receivers it is seldom practical to install enough stations to capture the full range of potential deformation modes. These limitations notwithstanding, a combination of InSAR, continuous GPS (or strainmeters, tiltmeters, etc.), and conventional geodetic techniques can provide important information about magma movements beneath volcanoes in space and time, thereby supporting better short-term assessments of hazards and in some cases extending the warning time before hazardous eruptions.

4. Summary

The study of ground deformation near hazardous volcanoes would seem to hold tremendous potential, because magma must accumulate beneath a volcano before it erupts and in so doing almost surely deforms the ground surface. A complete characterization of the surface displacement field in space and time would include information about the location, volume, and geometry of a subsurface magma body—information that could be used in conjunction with results from other types of studies to better assess and mitigate volcano hazards.

However, measurements of ground deformation at many of the world's dangerous volcanoes have so far been elusive, for reasons including difficult logistics, generally long repose periods, limited resources, and the likely complexity of displacement fields produced by magma moving through a heterogeneous crust. Point-to-point geodetic measurements (e.g. EDM, GPS) and *in situ* sensors (e.g. tiltmeters, strainmeters) alone, especially if the resulting data are sparse in space or time (as is usually the case), are simply not up to the task. Numerical modelling clearly shows that, in

† The Yellowstone continuous GPS network is a joint project involving the University of Utah (Yellowstone Hotspot Geodynamics project), the US Geological Survey (Volcano Hazards Program), and the University NAVSTAR Consortium (UNAVCO).

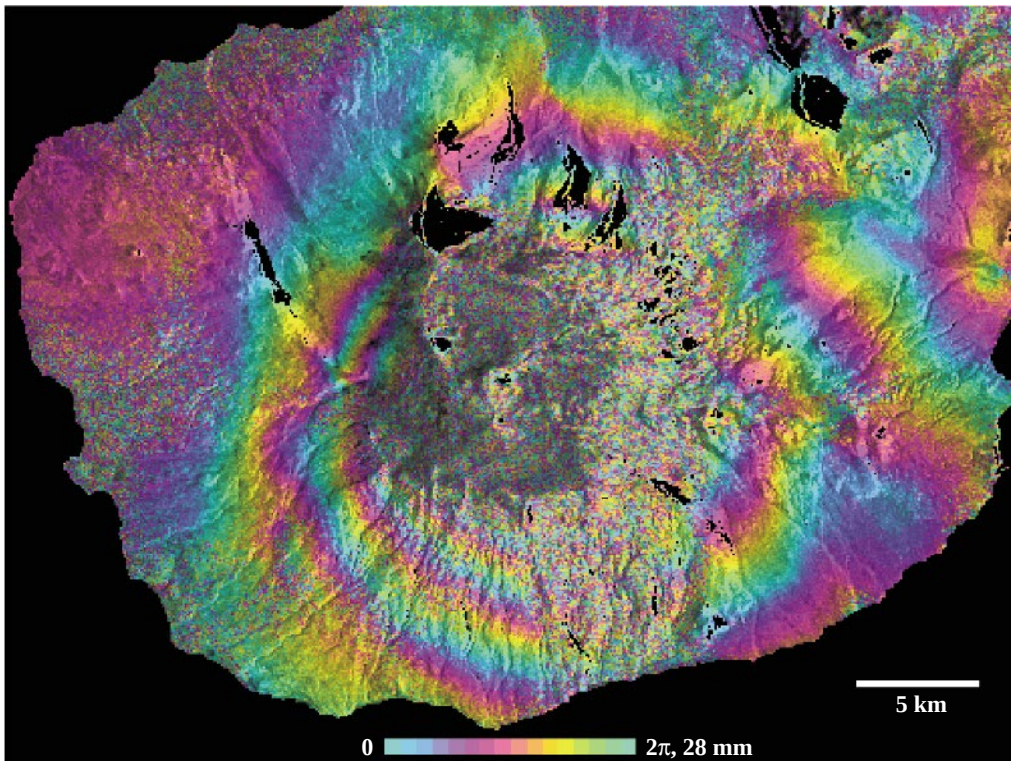

Figure 7. Displacement interferogram for Westdahl volcano, west part of Unimak Island, Alaska, for the period 1993–98, from Lu *et al.* (2000*b*). Colour scheme is the same as for figures 5 and 6 (i.e. the repeating blue–green–yellow–red sequence indicates uplift of the upper part of the volcano). Westdahl Peak, the historically active vent, is near the centre of the image. North is at the top. A preliminary model of the displacement field includes a spherical source 8 km deep that inflated by 0.05 km^3 during the interval spanned by the interferogram.

order to distinguish among the full range of possible source locations and geometries, especially if multiple sources might be present, it is necessary to make measurements virtually 'everywhere, all the time.' Fortunately, InSAR and continuous GPS represent large strides in that direction that can be applied at many of the world's volcanoes.

That said, it is also important to recognize that neither InSAR nor GPS will be useful in every volcano crisis situation. This is because limited sky visibility, especially from dense vegetation that occurs on many of the world's volcanoes, hinders both techniques. In addition, InSAR is subject to surface decorrelation caused by such common occurrences as precipitation, vegetation growth, and ashfall. Also, topographical errors and local perturbations in the ionosphere or troposphere can produce artefacts in interferograms that could be mistaken for surface deformation. Finally, the minimum orbital repeat times for existing InSAR satellites are too long to be useful during a rapidly evolving volcano crisis. For the foreseeable future, obtaining geodetic information 'everywhere, all the time' will require the use of several complementary geodetic techniques. Volcano geodesy's potential has yet to be

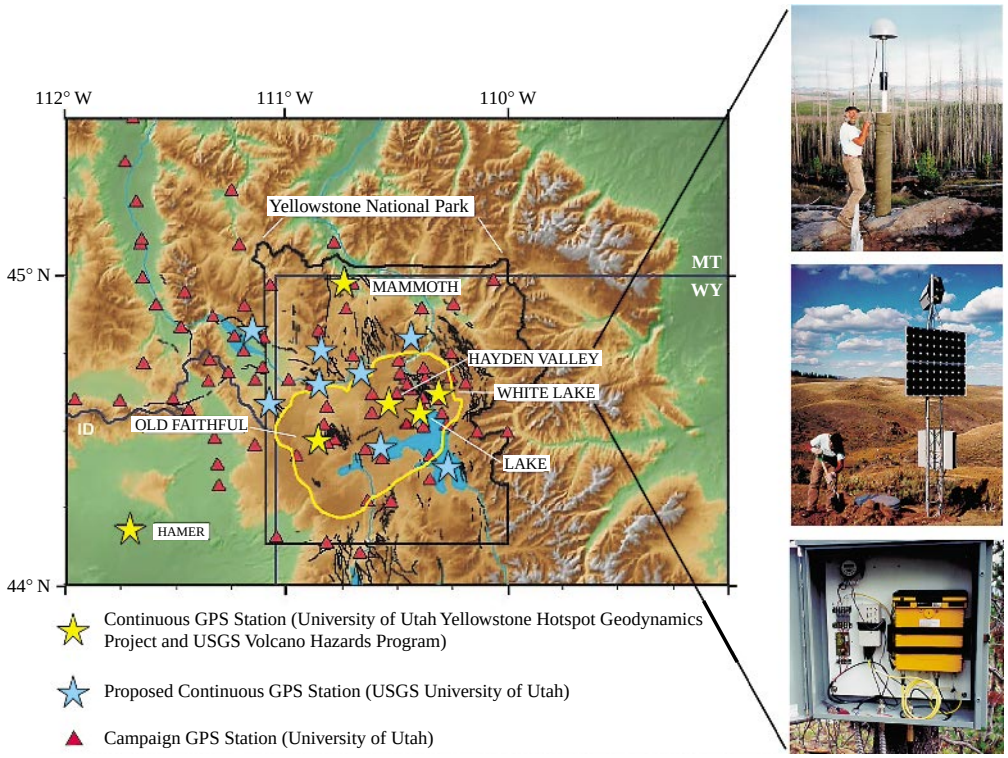

Figure 8. Campaign (triangles) and continuous (stars, existing and planned) GPS stations near Yellowstone National Park, including four continuous stations operating within Yellowstone caldera (yellow outline). Photographs at right: top, GPS monument and antenna at White Lake; middle, solar panels, telemetry antenna, and GPS receiver housing at Hayden Valley; bottom, detail of White Lake receiver housing, including Trimble 4000SSi receiver and Freewave radio modem. US Geological Survey photos by D. Dzurisin. Base map courtesy of R. B. Smith, University of Utah.

fully tapped, but recent results hint at the possibility of achieving fundamental new insights into intrusive processes beneath volcanoes in the not-too-distant future.

This work was supported by the US Geological Survey's Volcano Hazards Program. My colleagues Zhong Lu, Wayne Thatcher, and Charles Wicks supplied unpublished interferograms, modelling results, and consistently good counsel. I am indebted to The Royal Society for the opportunity to present this paper at the Discussion Meeting, and to reviewers Cynthia Gardner, Evelyn Roeloffs, and Geoff Wadge for their thoughtful reviews, which significantly improved the manuscript.

References

Delaney, P. T. & McTigue, D. F. 1994 Volume of magma accumulation or withdrawal estimated from surface uplift or subsidence, with application to the 1960 collapse of Kilauea Volcano. *Bull. Volcanol.* **56**, 417–424.

Dvorak, J. J. & Dzurisin, D. 1997 Volcano geodesy: the search for magma reservoirs and the formation of eruptive vents. *Rev. Geophys.* **35**, 343–384.

Dzurisin, D., Yamashita, K. M. & Kleinman, J. W. 1994 Mechanisms of crustal uplift and subsidence at the Yellowstone caldera, Wyoming. *Bull. Volcanol.* **56**, 261–270.

Dzurisin, D., Wicks Jr, C. & Thatcher, W. 1999 Renewed uplift at the Yellowstone caldera measured by leveling surveys and satellite radar interferometry. *Bull. Volcanol.* **61**, 349–355.

Gerlach, T. M., Westrich, H. R. & Symonds, R. B. 1996 Pre-eruption vapor in magma of the climactic Mount Pinatubo eruption: source of giant stratospheric sulfur dioxide cloud. In *Fire and mud: eruptions and lahars of Mount Pinatubo, Philippines* (ed. C. G. Newhall & R. S. Punongbayan), pp. 415–433. Quezon City: Philippine Institute of Volcanology and Seismology. Seattle and London: University of Washington Press.

Lejeune, A. M., Bottinga, Y., Trull, T. W. & Richet, P. 1999 Rheology of bubble-bearing magmas. *Earth Planet. Sci. Lett.* **166**, 71–84.

Linde, A. T., Agustsson, K., Sacks, I. S. & Stefansson, R. 1993 Mechanism of the 1991 eruption of Hekla from continuous borehole strain monitoring. *Nature* **365**, 737–740.

Lipman, P. W., Moore, J. G. & Swanson, D. A. 1981 Bulging of the north flank before the May 18 eruption—geodetic data. In *The 1980 eruptions of Mount St. Helens, Washington* (ed. P. W. Lipman & D. R. Mullineaux), pp. 143–155. US Geological Survey Professional Paper 1250.

Lu, Z., Wicks Jr, C., Power, J. A. & Dzurisin, D. 2000*a* Ground deformation associated with the March 1996 earthquake swarm at Akutan volcano, Alaska, revealed by satellite radar interferometry. *J. Geophys. Res.* (Submitted.)

Lu, Z., Wicks Jr, C. & Dzurisin, D. 2000*b* Aseismic inflation of Westdahl volcano, Alaska, detected by satellite radar interferometry. *Geophys. Res. Lett.* (In the press.)

McTigue, D. F. 1987 Elastic stress and deformation near a finite spherical magma body: resolution of the point source paradox. *J. Geophys. Res.* **92**, 12 931–12 940.

Massonnet, D. & Feigl, K. L. 1998 Radar interferometry and its application to changes in the Earth's surface. *Rev. Geophys.* **36**, 441–500.

Massonnet, D., Rossi, M., Carmona, C., Adragna, F., Peltzer, G., Feigl, K. & Rabaute, T. 1993 The displacement field of the Landers earthquake mapped by radar interferometry. *Nature* **364**, 138–142.

Miller, T. P., McGimsey, R. G., Richter, D. H., Riehle, J. R., Nye, C. J., Yount, M. E. & Dumoulin, J. A. 1998 Catalog of the historically active volcanoes of Alaska. US Geological Survey Open-File Report 98-582.

Mogi, K. 1958 Relation between the eruptions of various volcanoes and the deformation of the ground surfaces around them. *Bull. Earthqu. Res. Inst. Univ. Tokyo* **36**, 99–134.

Pallister, J. S., Hoblitt, R. P., Crandell, D. R. & Mullineaux, D. R. 1992 Mount St. Helens a decade after the 1980 eruptions: magmatic models, chemical cycles, and a revised hazards assessment. *Bull. Volcanol.* **54**, 126–146.

Richter, D. H., Waythomas, C. F., McGimsey, R. G. & Stelling, P. L. 1998 Geologic map of Akutan Island, Alaska. US Geological Survey Open-File Report 98-135.

Rutherford, M. J., Sigurdsson, H., Carey, S. & Davis, A. 1985 The May 18, 1980, eruption of Mount St. Helens. 1. Melt composition and experimental phase equilibria. *J. Geophys. Res.* **90**, 2929–2947.

Scandone, R. & Malone, S. D. 1985 Magma supply, magma discharge and readjustment of the feeding system of Mount St. Helens during 1980. *J. Volcanol. Geotherm. Res.* **23**, 239–262.

Simkin, T. & Siebert, L. 1994 *Volcanoes of the world*, 2nd edn. Tucson: Geoscience Press.

Wicks Jr, C., Thatcher, W. & Dzurisin, D. 1998 Migration of fluids beneath Yellowstone Caldera inferred from satellite radar interferometry. *Science* **282**, 458–462.